PROCEEDINGS OF SCIENCE

Determination of the strong coupling and its running from measurements of inclusive jet production at CMS

PoS(EPS-HEP2025)233

Valentina Guglielmi[1,*]

University of Zurich (UZH),
Rämistrasse 42, Zurich, Switzerland

E-mail: valentina.guglielmi@cern.ch

The value of the strong coupling α_S is determined in a comprehensive analysis at next-to-next-to-leading order accuracy in quantum chromodynamics. The analysis uses double-differential cross section measurements from the CMS Collaboration at the CERN LHC of inclusive jet production in proton-proton collisions at centre-of-mass energies of 2.76, 7, 8, and 13 TeV, combined with inclusive deep-inelastic data from HERA. The value $\alpha_S(m_Z) = 0.1176^{+0.0014}_{-0.0016}$ is obtained at the scale of the Z boson mass. By using the measurements in different intervals of jet transverse momentum, the running of α_S is probed for energies between 100 and 1600 GeV.

European Physical Society Conference on High Energy Physics 2025, EPS2025
7-11 July, 2025
Marseille, France

[1]On behalf of the CMS Collaboration
[*]Speaker

1. Introduction

The stability of the electroweak vacuum in the Standard Model (SM) remains an open question, and is driven by the values of the top quark mass, strong coupling constant $\alpha_S(m_Z)$ and, to a smaller extent, the Higgs boson mass. A more accurate and precise determination of $\alpha_S(m_Z)$ therefore plays a central role in constraining scenarios of vacuum stability within the SM.

Jets, abundantly produced in proton–proton (pp) collisions at the LHC, play a central role in this context. Predictions of jet production in pp collisions depend on the value of the strong coupling α_S and parton distribution functions (PDFs) of the proton. High precision jet measurements allow for the extraction of $\alpha_S(m_Z)$ and offer strong constraints on the PDFs at large values of the proton momentum fraction x carried by the struck parton. For sufficiently large transverse momenta p_T, jet production is reliably described within perturbative QCD, for which next-to-next-to-leading order (NNLO) predictions are now available. In particular, inclusive jet production (pp $\rightarrow$ jet + X) corresponds to events containing at least one jet above a given p_T threshold and constitutes a key benchmark for testing perturbative QCD calculations up to the highest energy scales.

These proceedings report a determination of $\alpha_S(m_Z)$ obtained in a simultaneous fit with PDFs in a comprehensive QCD analysis at NNLO. The analysis combines CMS [1, 2] measurements of inclusive jet production in pp collisions at centre-of-mass energies $\sqrt{s}$ =2.76, 7, 8, and 13 TeV with cross section measurements of inclusive deep inelastic scattering (DIS) from HERA [3]. The simultaneous extraction of $\alpha_S(m_Z)$ and PDFs mitigates their correlation and prevents potential biases in the determination of $\alpha_S(m_Z)$ [4]. Furthermore, the running of α_S is illustrated at NNLO up to an energy scale of 1.6 TeV. The results have been published in Ref. [5].

2. The data: CMS inclusive jet measurements

The four CMS measurements of the double-differential inclusive jet cross section as functions of the individual jet p_T and absolute rapidity $|y|$ at $\sqrt{s}$ =2.76, 7, 8, and 13 TeV are considered in these proceedings. In these measurements, the jets are clustered with the anti-k_T [6] algorithm as implemented in the FastJet [7] program with a radius of $R = 0.7$. The combination of the four measurements not only provides the highest statistical precision but also ensures coverage of a wider phase-space region. The integrated luminosity $\mathcal{L}$, the number of data points N_{dp}, and the intervals in p_T and $|y|$ of each measurement are listed in Table 1.

Table 1: Summary of the main characteristics of the CMS inclusive jet datasets used in these proceedings, together with the corresponding publications.

$\sqrt{s}$ [TeV]	$\mathcal{L}$ [fb^{-1}]	N_{dp}	p_T[GeV]	$\|y\|$	Ref.
2.76	0.0054	80	74–592	0.0–3.0	[12]
7	5.0	130	114–2116	0.0–2.5	[13, 14]
8	20	165	74–1784	0.0–3.0	[15]
13	33.5	78	97–3103	0.0–2.0	[16]

Furthermore, the systematic uncertainties have been re-evaluated and, for the first time, the correlations among the jet measurements have been thoroughly investigated. These updated systematics and correlations are included in the QCD analysis, resulting in a more precise and accurate determination of $\alpha_s(m_Z)$. The outcomes of these studies have been released publicly and provide valuable input for future global QCD analyses incorporating CMS inclusive jet data. A comprehensive description of the correlation scheme applied to the CMS measurements used in this work, along with the systematic re-evaluation, can be found in Ref. [5].

3. Theoretical predictions

The NNLO predictions for inclusive jet production used in this analysis are obtained with the NNLOJET program [8–10], computed with five active massless quark flavours in the leading-colour and leading-flavour-number approximations. The renormalization (μ_r) and factorisation (μ_f) scales are set to the p_T of each jet, following Ref. [9]. The differential cross sections in p_T and $|y|$ are provided through APPLFAST interpolation grids [11], which permit fast evaluation of the predictions under variations of $\alpha_S(m_Z)$, the PDFs, and the scale choices.

To compare the fixed-order predictions with the measured particle-level cross sections, the theoretical predictions are corrected for nonperturbative (NP) effects arising from hadronisation and the underlying event. These NP corrections are obtained as ratios of cross sections from parton-shower event generators, where NP effects are alternately switched on and off. The NP corrections published with the individual CMS measurements [12, 14–16] are used in this analysis and are most significant at low jet (p_T).

In addition, the QCD predictions are corrected for electroweak (EW) effects arising from the virtual exchanges of soft or collinear massive weak bosons, computed at next-to-leading order [17]. The magnitude of the EW corrections increases with jet p_T, reaching about 11% at the highest p_T values in the 13 TeV measurement. The EW corrections are taken from the original publication [16] for the 13 TeV dataset, while updated corrections based on more recent PDF sets are used for the 7 and 8 TeV measurements. No EW corrections are applied to the 2.76 TeV data, where their impact is negligible.

4. The QCD analysis

The simultaneous determination of $\alpha_S(m_Z)$ and PDFs is carried out using the four CMS jet measurements described in Section 2, together with the neutral-current and charged-current electron–proton DIS cross sections measured at HERA [3]. The NNLO predictions for jet production are discussed in Section 3, while the DIS cross sections are calculated at fixed order in QCD at NNLO using the QCDNUM program [18], with both μ_r and μ_f set to the squared four-momentum transfer Q^2. Heavy-flavour (c and b) contributions to the DIS cross sections are treated within the Thorne–Roberts general-mass variable-flavour number scheme [19–21]. The pole masses of the c and b quarks are fixed to $m_\mathrm{c} = 1.47\,\mathrm{GeV}$ and $m_\mathrm{b} = 4.5\,\mathrm{GeV}$, respectively. To avoid the tension between the low- and high-Q^2 regions reported in the original publication [3], only DIS data with $Q^2 > 10\,\mathrm{GeV}^2$ are included in the fit.

The PDFs for the gluon g, valence u- and d-quark, and $\overline{\mathrm{u}}$ and $\overline{\mathrm{d}}$ quark densities are parametrized at a starting evolution scale $Q_0^2 = 1.9\,\mathrm{GeV}^2$. The Q^2 evolution of both the PDFs and α_S is obtained by solving the DGLAP evolution equations at NNLO accuracy in perturbative QCD as implemented

PoS(EPS-HEP2025)233

in QCDNUM. The functional forms of the PDFs at the starting scale are:

$$x\mathrm{g}(x) = A_{\mathrm{g}} x^{B_{\mathrm{g}}} (1-x)^{C_{\mathrm{g}}} (1 + D_{\mathrm{g}} x + E_{\mathrm{g}} x^2), \tag{1}$$

$$x\mathrm{u}_v(x) = A_{\mathrm{u}_v} x^{B_{\mathrm{u}_v}} (1-x)^{C_{\mathrm{u}_v}} (1 + E_{\mathrm{u}_v} x^2), \tag{2}$$

$$x\mathrm{d}_v(x) = A_{\mathrm{d}_v} x^{B_{\mathrm{d}_v}} (1-x)^{C_{\mathrm{d}_v}}, \tag{3}$$

$$x\overline{\mathrm{u}}(x) = A_{\overline{\mathrm{u}}} x^{B_{\overline{\mathrm{u}}}} (1-x)^{C_{\overline{\mathrm{u}}}} (1 + D_{\overline{\mathrm{u}}} x), \tag{4}$$

$$x\overline{\mathrm{d}}(x) = A_{\overline{\mathrm{d}}} x^{B_{\overline{\mathrm{d}}}} (1-x)^{C_{\overline{\mathrm{d}}}} (1 + E_{\overline{\mathrm{d}}} x^2), \tag{5}$$

Here, the A_i denote normalisation parameters, while the polynomial factors $(1 + D_i x + E_i x^2)$ interpolate between the small- and large-x regimes governed by the parameters B_i and C_i. The D_i and E_i terms are included only following the results of an optimization procedure. The relations $x\overline{\mathrm{U}}(x) = x\overline{\mathrm{u}}(x)$ and $x\overline{\mathrm{D}}(x) = x\overline{\mathrm{d}}(x) + x\overline{\mathrm{s}}(x)$ are assumed for the up, down, and strange antiquarks $x\overline{\mathrm{u}}(x)$, $x\overline{\mathrm{d}}(x)$, and $x\overline{\mathrm{s}}(x)$. The sea quark distribution is defined as $x\Sigma(x) = 2x\overline{\mathrm{u}}(x) + x\overline{\mathrm{d}}(x) + x\overline{\mathrm{s}}(x)$. Following Ref. [3], the normalisations of $x\overline{\mathrm{u}}$ and $x\overline{\mathrm{d}}$ in the limit $x \to 0$ are taken to be identical by imposing $B_{\overline{\mathrm{U}}} = B_{\overline{\mathrm{D}}}$ and $A_{\overline{\mathrm{U}}} = A_{\overline{\mathrm{D}}}(1 - f_{\mathrm{s}})$. The strangeness fraction is fixed to $f_{\mathrm{s}} = \overline{\mathrm{s}}/(\overline{\mathrm{d}} + \overline{\mathrm{s}}) = 0.4$, consistent with Ref. [3].

The fit is performed using the open-source xFitter framework [22, 23], in which the PDFs and $\alpha_S(m_{\mathrm{Z}})$ are determined through a minimization procedure based on MINUIT [24]. The χ^2 goodness-of-fit function implemented in xFitter [22, 23] incorporates experimental systematic uncertainties via nuisance parameters. Asymmetric uncertainties on the PDF and $\alpha_S(m_{\mathrm{Z}})$ parameters are obtained using the $\Delta\chi^2 = 1$ criterion, following the method described in Ref. [25].

Following the HERAPDF strategy [3], several sources of uncertainty are included in the NNLO QCD fit in addition to the intrinsic fit uncertainty. The *scale uncertainty* is evaluated by varying μ_{r} and μ_{f} independently by factors of 2, excluding the configurations with $\mu_{\mathrm{f}}/\mu_{\mathrm{r}} = 4$ or 1/4. A separate fit is performed for each scale choice, and the largest deviation from the central result is taken as the uncertainty. The *model uncertainty* is obtained by varying the input parameters (such as minimum Q^2 for DIS data, m_{b}, m_{c}, f_{s} and Q_0^2) within their respective uncertainties. The *parametrisation uncertainty* is estimated by extending the PDF functional form with additional parameters (D or E), added one at a time, and taking the envelope of the resulting fits. The *total uncertainty* is then computed by adding in quadrature the fit, model, and scale components, and summing the parametrisation contribution linearly.

5. Results

The comparison between the data and the post-fit theoretical predictions is shown in Fig. 1. Overall, a very good agreement is observed. The consistency of all the experimental data is quantified through the goodness of the fit χ^2. Table 2 lists the values of χ^2 per $\mathrm{N_{dp}}$ for the individual data sets (partial $\chi^2/\mathrm{N_{dp}}$), along with the total χ^2 per number of degrees of freedom $\mathrm{N_{dof}}$, which is 1680/1453. A slightly higher partial $\chi^2/\mathrm{N_{dp}}$ for the HERA DIS data is consistent with the findings of the original work [3], and arises from tensions between measurements at low Q^2 ($< 15\,\mathrm{GeV}^2$) and high Q^2 ($> 150\,\mathrm{GeV}^2$). For the CMS jet measurements, the sum of the partial $\chi^2/\mathrm{N_{dp}}$ values, including correlations, is 496/453.

PoS(EPS-HEP2025)233

Table 2: The values of χ^2 per $\mathrm{N_{dp}}$ for each individual data set as obtained in the fit to HERA and CMS jet data, together with the contribution to the χ^2 from correlated uncertainty sources. In the last line, the total χ^2 per number of degrees of freedom, $\mathrm{N_{dof}}$, is reported.

Data set	Partial $\chi^2/\mathrm{N_{dp}}$
HERA I+II neutral current	1036/935
HERA I+II charged current	112/81
CMS jets 2.76 TeV	63/80
CMS jets 7 TeV	81/130
CMS jets 8 TeV	206/165
CMS jets 13 TeV	77/78
Correlated χ^2HERA	56
Correlated χ^2Jets	69
Total $\chi^2/\mathrm{N_{dof}}$	1680/1453

Figure 2 illustrates the impact of the CMS jet data on the extracted PDFs in the *HERA+CMS* fit, showing the corresponding 68% confidence-level (CL) uncertainties. These results are compared with those from a reference fit based solely on the HERA DIS measurements (*HERA-only* fit). In the latter case, the value of $\alpha_S(m_Z)$ is fixed to that obtained in the combined fit, since the DIS data alone provide limited sensitivity to $\alpha_S(m_Z)$. The PDFs are evaluated at the factorization scale $Q^2 = m_\mathrm{t}^2$, with m_t denoting the top-quark mass. Including the CMS jet measurements leads to a substantial reduction in the uncertainties of all PDFs. While previous analyses based on individual CMS jet datasets already indicated a significant improvement in the gluon distribution, the simultaneous use of all CMS inclusive jet measurements at several $\sqrt{s}$ also enhances the constraints on the $\mathrm{d_v}$ distribution.

The strong coupling constant, extracted simultaneously with the PDFs, results in:

$$\alpha_S(m_Z) = 0.11759^{+0.0009}_{-0.0009}\,(\mathrm{fit})^{+0.0006}_{-0.0004}\,(\mathrm{model})^{+0.0009}_{-0.0012}\,(\mathrm{scale})^{+0.}_{<-0.0001}\,(\mathrm{param.}), \tag{6}$$

with a total uncertainty of $^{+0.0014}_{-0.0016}$ (tot). The extracted value is consistent with the PDG world average of $\alpha_S(m_Z) = 0.1180 \pm 0.0009$ [26] and represents the most precise determination obtained by CMS to date, as shown in Fig. 3 (right), and from jets at the LHC.

Furthermore, the running of the strong coupling, $\alpha_S(\mu_\mathrm{r})$, is probed by extracting α_S in five distinct ranges of the renormalization scale defined by $\mu_\mathrm{r} = p_\mathrm{T}$. For this purpose, the CMS inclusive jet measurements are divided into exclusive intervals of individual jet p_T. A dedicated fit of the PDFs and $\alpha_S(m_Z)$ is then carried out independently within each p_T range. The resulting values of $\alpha_S(m_Z)$ are evolved to $\alpha_S(\mu_\mathrm{r})$ using the five-loop five-flavour renormalization group equation (RGE) implemented in CRunDec [27], which is also used to propagate the associated uncertainties. The fit, model, scale, and parametrization uncertainties are evaluated following the same procedure as for Eq. (6). For each p_T range, the corresponding scale μ_r is defined as the NNLO cross-section-weighted average $\langle p_\mathrm{T} \rangle$. The extracted values of $\alpha_S(\mu_R)$ are displayed in Fig. 3 and compared with the five-loop QCD evolution of the world-average $\alpha_S(m_Z)$, computed using CRunDec. The running of α_S is tested at NNLO in QCD up to energy scales of 1.6 TeV and is in agreement with the prediction of the QCD renormalization group equation.

PoS(EPS-HEP2025)233

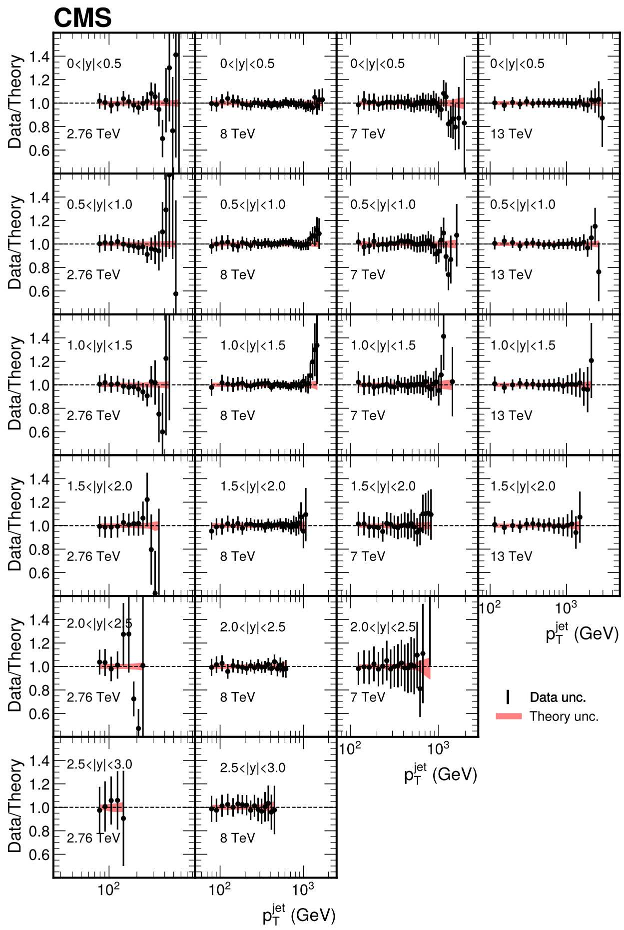

Figure 1: Cross section ratios between data and post-fit theory predictions as functions of individual jet p_T in intervals of absolute rapidity $|y|$. Shown are the total uncertainties of each data point and the total theoretical uncertainty, which includes contributions from PDF and scale variations. The PDFs obtained in this work are used. From Ref. [5].

6. Summary and conclusions

The stability of the electroweak vacuum remains an open question, and its investigation is closely connected to the precise values of the top-quark mass and the strong coupling constant. Improving the precision of these two SM parameters, therefore, provides more stringent constraints on the electroweak vacuum stability. These proceedings report the most precise determination of $\alpha_S(m_Z)$ from jet cross sections to date, obtained by combining CMS inclusive jet measurements at $\sqrt{s}$ = 2.76, 7, 8 and 13 TeV. A simultaneous fit of $\alpha_S(m_Z)$ and PDFs at NNLO accuracy yields $\alpha_S(m_Z) = 0.1176^{+0.0014}_{-0.0016}$, in good agreement with the world average. In addition, the running of α_S is illustrated at NNLO up to energy scales of 1.6 TeV.

PoS(EPS-HEP2025)233

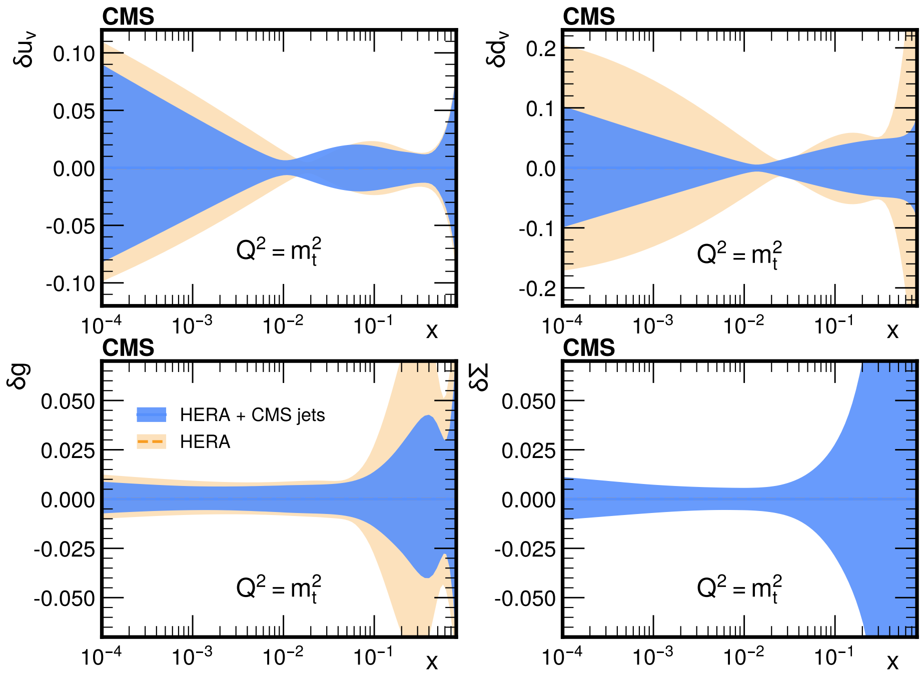

Figure 2: The fit uncertainties at 68% CL in the u_v (upper left), d_v (upper right), g (lower left), and Σ (lower right) distributions, shown as a function of x. The results of the HERA+CMS fit are compared with the results of the HERA-only fit. From Ref. [5].

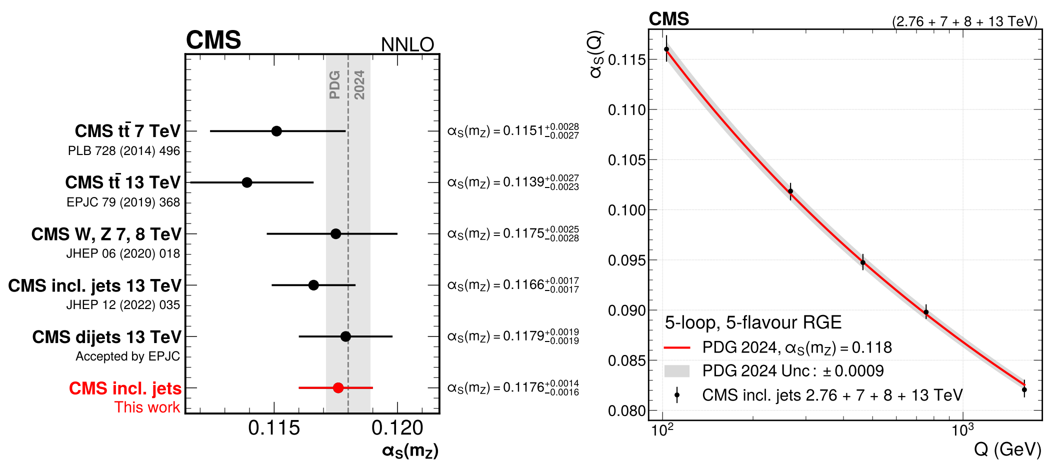

Figure 3: Left: The value of $\alpha_S(m_Z)$ obtained in this analysis compared with all CMS results at NNLO with their total uncertainties. The PDG world average, together with its uncertainty, is also shown. From Ref. [5]. Right: Illustration of the α_S running at NNLO accuracy. For comparison, the RGE at 5 loops is shown using the current world-average value $\alpha_S(m_Z)$ [26] together with its associated total uncertainty. From Ref. [5].

References

[1] CMS Collaboration, *The CMS experiment at the CERN LHC* JINST, **3**, (2008) S08004.

[2] CMS Collaboration, *Development of the CMS detector for the CERN LHC Run 3*, JINST, **19**, (2024) P05064 [arXiv:2309.05466].

[3] H1 and ZEUS Collaborations, *Combination of measurements of inclusive deep inelastic $e^{\pm}p$ scattering cross sections and QCD analysis of HERA data*, Eur. Phys. J. C **75** (2015) 580 [arXiv:1506.06042].

[4] S. Forte and Z. Kassabov, *Why α_s cannot be determined from hadronic processes without simultaneously determining the parton distributions*, Eur. Phys. J. C **80** (2020) 182 [arXiv:2001.04986].

[5] CMS Collaboration, *Determination of the strong coupling and its running from measurements of inclusive jet production*, Phys. Lett. B **868** (2025) 139651 [arXiv:2412.16665].

[6] M. Cacciari, G. P. Salam, and G. Soyez, *The anti-k_{T} jet clustering algorithm*, JHEP **04** (2008) 063 [arXiv:0802.1189].

[7] M. Cacciari, G. P. Salam, and G. Soyez, *FastJet user manual*, Eur. Phys. J. C **72** (2012) 1896 [arXiv:1111.6097].

[8] J. Currie, E. W. N. Glover, and J. Pires, *Next-to-next-to leading order QCD predictions for single jet inclusive production*, Phys. Rev. Lett. **118** (2017) 072002 [arXiv:1611.01460].

[9] J. Currie *et al.*, *Infrared sensitivity of single jet inclusive production*, JHEP **10** (2018) 155 [arXiv:1807.03692].

[10] T. Gehrmann *et al.*, *Jet cross sections and transverse momentum distributions with NNLOJET*, *PoS RADCOR2017* (2018) 074 [arXiv:1801.06415].

[11] D. Britzger *et al.*, *NNLO interpolation grids for jet production at the LHC*, Eur. Phys. J. C **82** (2022) 930 [arXiv:2207.13735].

[12] CMS Collaboration, *Measurement of the inclusive jet cross section in pp collisions at $\sqrt{s}$ = 2.76 TeV*, Eur. Phys. J. C **76** (2016) 265 [arXiv:1512.06212].

[13] CMS Collaboration, *Measurements of differential jet cross sections in proton–proton collisions at $\sqrt{s}$ = 7 TeV*, Phys. Rev. D **87** (2013) 112002 [arXiv:1212.6660].

[14] CMS Collaboration, *Constraints on parton distribution functions and extraction of the strong coupling constant from the inclusive jet cross section at 7 TeV*, Eur. Phys. J. C **75** (2015) 288 [arXiv:1410.6765].

[15] CMS Collaboration, *Measurement and QCD analysis of double-differential inclusive jet cross sections at $\sqrt{s}$ = 8 TeV*, JHEP **03** (2017) 156 [arXiv:1609.05331].

[16] CMS Collaboration, *Measurement and QCD analysis of double-differential inclusive jet cross sections at $\sqrt{s} = 13$ TeV*, *JHEP* **02** (2022) 142 [arXiv:2111.10431] [Addendum: JHEP 12 (2022) 035.]

[17] S. Dittmaier, A. Huss and C. Speckner, *Weak radiative corrections to dijet production*, *JHEP* **11** (2012) 095 [arXiv:1210.0438].

[18] M. Botje, *QCDNUM: Fast QCD evolution and convolution*, *Comput. Phys. Commun.* **182** (2011) 490 [arXiv:1005.1481].

[19] R. S. Thorne and R. G. Roberts, *Ordered analysis of heavy flavor production*, *Phys. Rev. D* **57** (1998) 6871 [arXiv:hep-ph/9709442].

[20] R. S. Thorne, *Variable-flavor number scheme for NNLO*, *Phys. Rev. D* **73** (2006) 054019 [arXiv:hep-ph/0601245].

[21] R. S. Thorne, *Effect of changes in VFNS on PDFs*, *Phys. Rev. D* **86** (2012) 074017 [arXiv:1201.6180].

[22] S. Alekhin *et al.*, *HERAFitter*, *Eur. Phys. J. C* **75** (2015) 304 [arXiv:1410.4412].

[23] xFitter Developers' Team, *xFitter 2.0.0*, *PoS DIS2017* (2018) 203 [arXiv:1709.01151].

[24] F. James and M. Roos, *Minuit - a system for function minimization and analysis of the parameter errors and correlations*, *Comput. Phys. Commun.* **10** (1975) 343.

[25] J. Pumplin *et al.*, *Uncertainties from PDFs: Hessian method*, *Phys. Rev. D* **65** (2001) 014013 [arXiv:hep-ph/0101032].

[26] Particle Data Group, *Review of Particle Physics*, *Phys. Rev. D* **110** (2024) 030001.

[27] F. Herren and M. Steinhauser, *RunDec/CRunDec v3*, *Comput. Phys. Commun.* **224** (2018) 333 [arXiv:1703.03751].

PoS(EPS-HEP2025)233